Tightly-Coupled INS, GPS, and Imaging Sensors for Precision Geolocation

M. Veth , *Air Force Institute of Technology*
R. Anderson, *National Geospatial-Intelligence Agency*
F. Webber, *Air Force Institute of Technology*
M. Nielsen, *Air Force Test Pilot School* *

BIOGRAPHY

Major Mike Veth is an Assistant Professor in the Department of Electrical and Computer Engineering at the Air Force Institute of Technology. His current research focus is on the fusion of optical and inertial systems. He received his Ph.D. in Electrical Engineering from the Air Force Institute of Technology, and a B.S. in Electrical Engineering from Purdue University. In addition, Major Veth is a graduate of the Air Force Test Pilot School.

Robert C. Anderson has been working for NGA (and its predecessor organizations) specializing in the geodetic science field for the last 18 years. He currently works in the Remote Sensing Division of NGA's Basic and Applied Research Office with a current focus on developing improved surveying and mapping tools and techniques. He has Master of Science degrees from The Ohio State University in Geodetic Science and Southern Illinois University in Mathematics, and is a Ph.D. candidate in Mathematics at St. Louis University.

Fred Webber is currently studying for a Master's degree in Electrical Engineering at the Air Force Institute of Technology. His research focus is in the area of estimation theory. He is a research assistant for the Advanced Navigation Technology Center. He received his Bachelor of Science in Mechanical Engineering and Computer Science from Rose-Hulman Institute of Technology and is a member of AIAA and the Institute of Navigation.

Captain Mike Nielsen is an experimental test pilot assigned to the Air Force Test Pilot School. He is currently studying for a Master's degree in Electrical Engineering at the Air Force Institute of Technology. He has logged over 1000 hours in the F-15E, F-16, T-38 and various other aircraft. Capt Nielsen is a graduate of the Air Force Test Pilot School.

*The views expressed in this article are those of the author and do not reflect the official policy or position of the United States Air Force, National Geospatial-Intelligence Agency, Department of Defense, or the U.S. Government.

ABSTRACT

Recent technological advances have significantly improved the capabilities of micro-air vehicles (MAV). This is evidenced by their expanding use by government, police, and military forces. A MAV can provide a real-time surveillance capability to even the smallest units, which provides commanders with a significant advantage.

This capability is a result of the availability of miniaturized autopilot systems which typically combine inertial, pitot-static, and GPS sensors into a feedback flight-control system. While these autopilots can provide an autonomous flight capability, they have some limitations which impact their operational effectiveness. One of the primary issues is poor image geolocation performance, which limits the use of these systems for direct measurements of target locations. This poor geolocation performance is primarily a consequence of the relatively large attitude errors characteristic of low-performance inertial sensors. In previous efforts, we have developed a tightly-coupled image-aided inertial navigation system to operate in areas not serviced by GPS. This system extracts navigation information by automatically detecting and tracking stationary optical features of opportunity in the environment. One characteristic of this system is vastly reduced attitude errors, even with consumer-grade inertial sensors.

In this paper, the benefits of incorporating image-based navigation techniques with inertial and GPS measurements is explored. After properly integrating GPS with the image-aided inertial architecture,

Report Documentation Page

Form Approved
OMB No. 0704-0188

1. REPORT DATE	2. REPORT TYPE	3. DATES COVERED
2008		**00-00-2008 to 00-00-2008**

4. TITLE AND SUBTITLE	5a. CONTRACT NUMBER
Tightly-Coupled INS, GPS, and Imaging Sensors for Precision Geolocation	5b. GRANT NUMBER
	5c. PROGRAM ELEMENT NUMBER
6. AUTHOR(S)	5d. PROJECT NUMBER
	5e. TASK NUMBER
	5f. WORK UNIT NUMBER
7. PERFORMING ORGANIZATION NAME(S) AND ADDRESS(ES) **Air Force Institute of Technology,Department of Electrical and Computer Engineering,Wright Patterson AFB,OH,45433**	8. PERFORMING ORGANIZATION REPORT NUMBER
9. SPONSORING/MONITORING AGENCY NAME(S) AND ADDRESS(ES)	10. SPONSOR/MONITOR'S ACRONYM(S)
	11. SPONSOR/MONITOR'S REPORT NUMBER(S)

12. DISTRIBUTION/AVAILABILITY STATEMENT
Approved for public release; distribution unlimited

13. SUPPLEMENTARY NOTES

14. ABSTRACT

Recent technological advances have significantly improved the capabilities of micro-air vehicles (MAV). This is evidenced by their expanding use by government, police, and military forces. A MAV can provide a real-time surveillance capability to even the smallest units, which provides commanders with a significant advantage. This capability is a result of the availability of miniaturized autopilot systems which typically combine inertial, pitot-static, and GPS sensors into a feedback flight-control system. While these autopilots can provide an autonomous flight capability, they have some limitations which impact their operational effectiveness. One of the primary issues is poor image geolocation performance, which limits the use of these systems for direct measurements of target locations. This poor geolocation performance is primarily a consequence of the relatively large attitude errors characteristic of low-performance inertial sensors. In previous efforts, we have developed a tightly-coupled image-aided inertial navigation system to operate in areas not serviced by GPS. This system extracts navigation information by automatically detecting and tracking stationary optical features of opportunity in the environment. One characteristic of this system is vastly reduced attitude errors, even with consumer-grade inertial sensors. In this paper, the benefits of incorporating image-based navigation techniques with inertial and GPS measurements is explored. After properly integrating GPS with the image-aided inertial architecture, the system is tested using a combination of Monte-Carlo simulation and flight test data. The flight test data was flown over Edwards AFB using representative hardware. The experimental results are compared with validated truth data. The effects of variations in sensor quality and integration methods are investigated and shown to greatly improve the overall performance of the tightly-coupled image-aided sensor over the reference GPS/INS sensor.

15. SUBJECT TERMS

16. SECURITY CLASSIFICATION OF:			17. LIMITATION OF ABSTRACT	18. NUMBER OF PAGES	19a. NAME OF RESPONSIBLE PERSON
a. REPORT **unclassified**	b. ABSTRACT **unclassified**	c. THIS PAGE **unclassified**	**Same as Report (SAR)**	**10**	

Standard Form 298 (Rev. 8-98)
Prescribed by ANSI Std Z39-18

the system is tested using a combination of Monte-Carlo simulation and flight test data. The flight test data was flown over Edwards AFB using representative hardware. The experimental results are compared with validated truth data. The effects of variations in sensor quality and integration methods are investigated and shown to greatly improve the overall performance of the tightly-coupled image-aided sensor over the reference GPS/INS sensor.

INTRODUCTION

Virtually all UAVs and aircraft are flying with electro-optical (EO), infrared (IR), or video cameras. Even the smallest can now be equipped with an integrated Global Positioning System (GPS) and inertial navigation system (INS). Unfortunately, there is a very limited set of vehicles that provide the level of navigation and timing precision to the imaging path sufficient for generating high-quality geospatial-intelligence products. This is due to a variety of reasons such as cost or payload restrictions that mandate small low cost inertial navigation systems; or, to difficulties in precise timing of the metadata to the epoch of the frame exposure; or, to the expense and complications involved with establishing accurate GPS positions using dual frequency phase difference processing with associated communications links.

In order to address the issue of poor georegistration performance for small uavs, a number of research projects have been conducted. The most prominent approaches address the issue in three primary ways. The first, and probably most obvious, approach is to simply improve the quality of the inertial and GPS sensors until the desired target location accuracy is achieved. The advantage of this approach is its simplicity. The disadvantages are the increased cost and weight requirements for improved sensors (especially gyroscopes) that make this approach of limited appeal for small UAV operations. A variation on this theme was proposed by Hirokawa [5] where three very low-cost GPS sensors with displaced antennas were used to greatly improve the attitude performance of the navigation sensor, resulting in improved geolocation accuracy. The second approach [1] utilizes previously-surveyed reference targets in the images to automatically update and correct the navigation errors in the UAV. This system has the capability to eliminate inertial sensor drift when the aircraft remains in an operations area with visible reference targets. The final approach uses post-flight image registration software to correct each image to a known set of ground control points. This process can be performed manually or automatically and tends to be used in an open-loop, postflight mode (i.e., navigation error estimates are not fed back to the vehicle for correction).

The motivation for this paper is to determine if the position and orientation of camera frames can be significantly improved by augmenting the camera navigation system with an image-aided algorithm that reliably tracks image features across frames in a robust manner. This implies that the image-aiding algorithms add to the solution across a wide variety of terrain types, thus allowing for additional estimates of the camera position and orientation in the dynamic adjustment. As an additional benefit, the system should be able to continue to navigate in the presence of GPS dropouts.

The proof of concept testing will involve both simulations and generation of accuracy estimates that will conclude with testing a MAV prototype flown over a test area with visible survey control points that will be compared to derived coordinates from the system. Additionally, Geo-TIFFs will be generated from the camera/MAV system and compared to control. The overall goal of the project is to deliver a prototype small-UAV imagery collection system to the National Geospatial-Intelligence Agency (NGA) for further testing and use in generating Geo-Intelligence and Geo-Security products. The purpose of this paper is to outline the method used to fuse the image, inertial, and GPS measurements with a simple terrain database. The algorithm is tested using Monte Carlo simulation and experimental flight data collected using prototype hardware. Results and lessons learned will be addressed and incorporated into future designs.

This paper is organized as follows. First, a development of the assumptions and sensor models regarding the specific problem of interest is presented. In addition, the extended Kalman filter used to tightly-couple the image tracking and GPS/INS functionality is described. Next, the performance of the integrated navigation technique is compared to the stand-alone GPS/INS technique using a Monte-Carlo simulation and flight test data. Finally, conclusions are drawn regarding the performance of the technique and future work is presented.

DEVELOPMENT

As mentioned in the previous section, the goal of this research effort is to investigate the navigation and target location accuracy improvements achievable by tightly integrating an image-based feature tracking algorithm with GPS and a consumer-grade inertial

sensor. In this section, the overall design of the extended Kalman filter [8, 9] is presented along with a description of the sensor models.

Assumptions

This method is based on the following assumptions.

- A strapdown inertial measurement unit (IMU) and GPS antenna are rigidly attached to one or more calibrated cameras. Synchronized raw measurements are available from all sensors.
- The inertial, GPS and optical sensors' relative position and orientation are known (see [13] for a discussion of boresight calibration procedures).
- The camera images areas in the environment which contain some stationary objects.
- A statistical terrain model is available which provides an initial indication of range to objects in the environment.

Reference Frames

In this paper, four reference frames are used. Variables expressed in a specific reference frame are indicated using superscript notation. The Earth-Centered Earth-Fixed (ECEF, or e frame) is a Cartesian system with the origin at the Earth's center, the $\hat{x}^e$ axis pointing toward the intersection of the equator and the prime (Greenwich) meridian, the $\hat{z}^e$ axis extending through the North pole, and the $\hat{y}^e$ axis is the orthogonal compliment (in this paper, a carat symbol, $\hat{}$, denotes a unit vector).

The Earth-fixed navigation frame (n-frame) is an orthonormal basis in $\Re^3$, with origin located at a predefined location on the Earth, typically very close to the current operations area. The Earth-fixed navigation frame's x, y, and z axes point in the north, east, and down (NED) directions relative to the origin, respectively. Down is defined as the direction of the nominal gravity vector at the origin. In contrast to the body-fixed navigation frame, the Earth-fixed navigation frame remains fixed to the surface of the Earth. While this frame is not useful for very-long distance navigation, it can simplify the navigation kinematic equations for local navigation routes and is especially appropriate for micro-air vehicle flight profiles. The Earth-fixed navigation frame is shown in Figure 1.

The vehicle body frame (or b frame) is a Cartesian system with origin at the vehicle center of gravity, the $\hat{x}^b$ axis extending through the vehicle's nose, the $\hat{y}^b$ axis extending through the vehicle's right side, and the $\hat{z}^b$ axis points orthogonally out the bottom of the vehicle. The inertial measurements are expressed in the b frame.

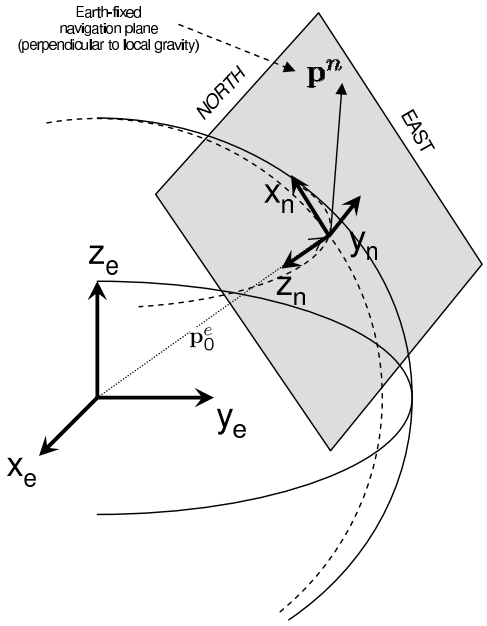

Figure 1: *Earth-fixed navigation frame. The Earth-fixed navigation frame is a Cartesian reference frame which is perpendicular to the gravity vector at the origin and fixed to the Earth.*

The camera frame (or c frame) is a Cartesian system with origin at the center of the camera image plane, the $\hat{x}^c$ axis is parallel to the camera image plane and defined as "camera up", the $\hat{y}^c$ axis is parallel to the camera image plane and defined as "camera right", and the $\hat{z}^c$ axis points out of the camera aperture, orthogonal to the image plane. The camera frame is shown in Fig. 2.

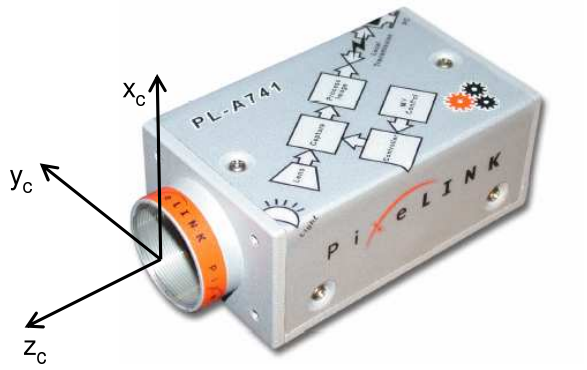

Figure 2: *Camera frame illustration. The camera reference frame originates at the optical center of the camera.*

Algorithm Description

The system parameters (see Table 1) consist of the navigation parameters (position, velocity, and attitude), inertial sensor biases, GPS clock bias and drift, and a vector describing the location of landmarks of interest ($\mathbf{t}^n$) in the navigation frame. The navigation parameters are calculated using body-frame velocity increment ($\Delta\mathbf{v}^b$) and angular increment ($\Delta\boldsymbol{\theta}^b_{ib}$) measurements from the inertial navigation sensor which have been corrected for bias errors using the current filter-computed bias estimates. These measurements are integrated from an initial state in the navigation (local-level) frame using mechanization algorithms described in [12].

Table 1: *System Parameter Definition*

Parameter	Description
$\mathbf{p}^n$	Vehicle position in navigation frame (northing, easting, and down)
$\mathbf{v}^n$	Vehicle velocity in navigation frame (north, east, down)
$\mathbf{C}^n_b$	Vehicle body to navigation frame DCM
$\mathbf{a}^b$	Accelerometer bias vector
$\mathbf{b}^b$	Gyroscope bias vector
$\mathbf{t}^n_m$	Location of landmark m in the navigation frame (one for each landmark currently tracked)
$\delta\mathbf{t}_{gps}$	GPS clock bias
$\delta\dot{\mathbf{t}}_{gps}$	GPS clock drift

The position, velocity, and attitude errors were modeled as a stochastic process based on the well-known Pinson navigation error model [12]. The accelerometer and gyroscopic bias errors were each modeled as a first-order Gauss-Markov process [8], based on the specification for the inertial measurement unit (IMU). The GPS clock drift is modeled as a random bias. The landmarks are modeled as stationary with respect to the Earth. A small amount of process noise is added to the state dynamics to promote filter stability [9].

EKF Mechanization

Because both the system dynamics model and measurement models are non-linear stochastic differential equations, an extended Kalman filter algorithm is employed. While other recursive estimation techniques have been proposed which have superior characteristics when dealing with non-linear models (e.g., unscented Kalman filters or particle filters [4]), the extended Kalman filter is still widely used for integrating inertial and GPS sensors.

In this paper, the extended Kalman filter is an error-state with feedback formulation which estimates the errors about the nominal trajectory produced by the nonlinear filter dynamics model. In addition, this nominal trajectory serves as the operating point where the nonlinear dynamics and measurement models are linearized [9]. Finally, the feedback nature attempts to constrain the inevitable departure of the nominal trajectory by periodically removing error estimates. This feedback process improves the performance of the extended Kalman filter by reducing linearization errors due to errors in the nominal trajectory. For more information regarding methods for integrating GPS and inertial sensors, see [11]. A block diagram of the system is shown in Figure 3.

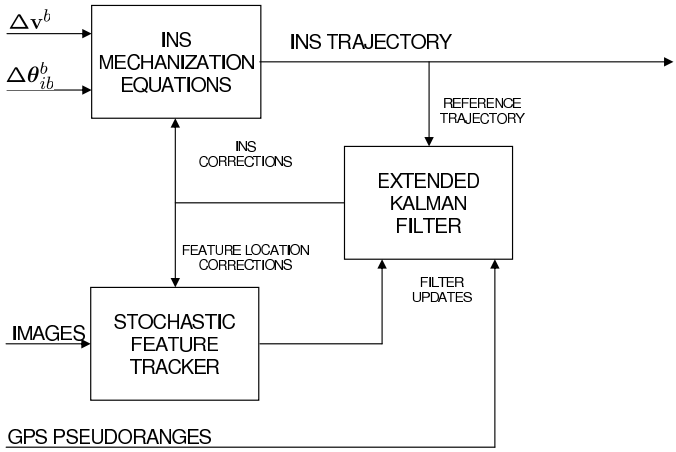

Figure 3: *Image-aided GPS/IMU navigation filter block diagram. In this filter, the location of stationary objects are tracked and used to estimate and update the errors in a GPS-aided inertial navigation system. The inertial navigation system is, in turn, used to support the feature tracking loop.*

GPS Model and Updates

The navigation filter is based on single-frequency pseudorange measurements, which can be corrected using a differential reference station at a surveyed location. A typical pseudorange measurement from the mobile receiver to satellite k is modeled by

$$\rho^k_m = \|\mathbf{p}^n_k - \mathbf{p}^n_m\| + c\delta t_{m_{gps}} + T^k_m + I^k_m + \nu_m + m_m \quad (1)$$

where $\mathbf{p}^n_k$ is the satellite location vector in the n-frame, $\mathbf{p}^n_m$ is the mobile receiver location vector in the n-frame, c is the speed of light, $\delta t_{m_{gps}}$ is the mobile receiver clock error, T^k_m is the tropospheric code delay from the mobile receiver to satellite k, I^k_m is the ionospheric code delay from the mobile receiver to satellite k, ν_m is the code measurement noise, and m_m is the code multipath.

The pseudorange measurement from the reference station to satellite k is modeled similarly as

$$\rho_r^k = \|\mathbf{p}_k^n - \mathbf{p}_r^n\| + c\delta t_{r_{gps}} + T_r^k + I_r^k + \nu_r + m_r \quad (2)$$

Because the reference station is at a known location, the equation can be rewritten as

$$\rho_r^k - \|\mathbf{p}_k^n - \mathbf{p}_r^n\| = c\delta t_{r_{gps}} + T_r^k + I_r^k + \nu_r + m_r \quad (3)$$

Subtracting (3) from (1) and grouping common error terms yields the differentially corrected pseudorange measurement

$$\rho_{corr}^k = \|\mathbf{p}_k^n - \mathbf{p}_m^n\| + c\delta t_{gps} + \Delta T^k + \Delta I^k + \nu + \Delta m \quad (4)$$

If the distance between the reference and mobile receivers is small, the differential atmospheric and satellite position errors become insignificant. Grouping the error terms into a common random variable, ν, yields the nonlinear measurement equation

$$\rho_{corr}^k = \|\mathbf{p}_k^n - \mathbf{p}_m^n\| + c\delta t_{gps} + \nu \quad (5)$$

Note this is of the general form

$$z = h\left[\mathbf{x}\right] + \nu \quad (6)$$

where $\mathbf{x}$ is the navigation state vector and ν is modeled as zero-mean additive white Gaussian noise with variance

$$\sigma_\nu^2 = E\left[\nu^2\right] \quad (7)$$

where $E\left[\cdot\right]$ is the expectation operator. For this simulation, a variance of $\sigma_\nu^2 = 2.6m^2$ was chosen as a conservative estimate of the pseudorange errors found in a consumer-grade, single-frequency GPS receiver. In the next section, the automatic feature detection and tracking algorithm is presented.

Automated Feature Tracking

Significant navigation information can be extracted by tracking stationary optical features over multiple images [14]. In order to accomplish this task, a number of issues must be addressed, namely, feature detection, feature correspondence matching, and correcting the navigation state. An overview of the image-aided inertial navigation algorithm is shown in Figure 4.

Feature detection is the process of automatically locating objects in an image and building some descriptor that allows the feature to be located in subsequent images. The optimal feature has three characteristics:

- easy to detect (i.e., *strong*)

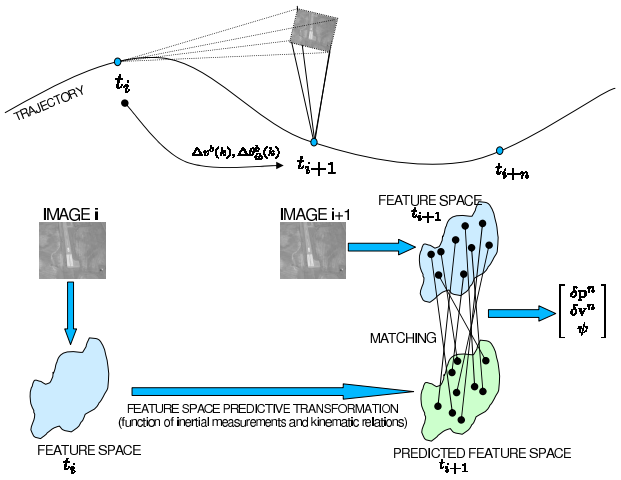

Figure 4: *Overview of image-aided inertial algorithm. Inertial measurements are used to aid the feature correspondence search which, in turn, is used to correct the navigation state.*

- unique (i.e., there exist significant differences which make this feature different from other features)
- ego-motion invariant (i.e., the feature descriptor does not change as a result of camera motion)

One popular algorithm that partially addresses these issues is Lowe's scale-invariant feature transformation (SIFT) [6]. The SIFT algorithm selects features which have a strong gradient in both x and y directions. Once the features are selected that meet the gradient threshold, a 128-byte descriptor is calculated such that it is invariant to rotation and scale changes. Additionally, the SIFT descriptor has been empirically shown to be distinct and appropriate for robust feature matching. One drawback of the SIFT algorithm is the features are only partially invariant to affine (i.e., perspective) changes. The other drawback of the SIFT algorithm is the computational complexity which can lead to difficulties implementing the algorithm in real-time. One solution to this issue is to leverage the use of general-purpose graphical processing units (GPGPU) to speed up the feature extraction task [3]. Our research has shown processing time reductions of up to 30x when using a GPU to extract robust features.

Once features of interest have been identified, the next step is to determine the correspondence between each feature and a matching feature in multiple images. When an inertial sensor is available, the method of employing stochastic constraints becomes attractive [15]. This technique is illustrated in Figure 5. The inertial measurements are used to statistically predict

the location of a current-image feature into a future image in order to reduce the search space and eliminate statistically-unlikely false matches.

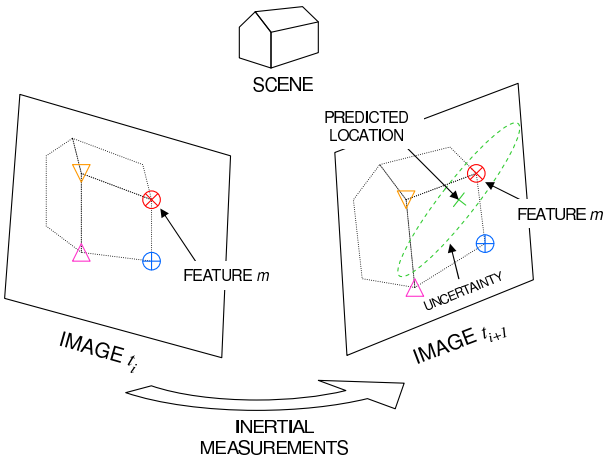

Figure 5: *Stochastic feature projection. Optical features of interest are mapped into future images using inertial measurements and stochastic projections.*

Once the correspondence has been determined between the predicted location of a feature and the measured location in the current image, the navigation state is corrected using a Kalman filter update. The update is calculated using the projected feature locations in Eqns. (8) and (9) with an additive, white Gaussian noise. The Jacobian of the nonlinear measurement is calculated about the nominal trajectory in terms of the system states described previously.

In the next section, the camera model is defined mathematically along with the feature extraction and tracking methodology.

Imaging Model and Updates

In addition to the GPS and inertial sensors, a digital camera is used to track features of interest. The first item of interest is the definition of the camera projection model. After properly compensating for the effects of nonlinear distortions (see [2] or [7]), the camera is modeled as a pin-hole device. The pin-hole camera model is shown in Figure 6. This implies that the location of a feature on the image plane is simply the projection of the true location vector of the feature expressed in the camera frame. Thus, given a point source at location $\mathbf{s}^c$ the resulting location of the point source in the image plane, relative to the optical center of the camera is given by

$$\mathbf{s}^{proj} = \left(\frac{f}{s_z^c}\right)\mathbf{s}^c \tag{8}$$

where s_z^c is the distance of the point source from the

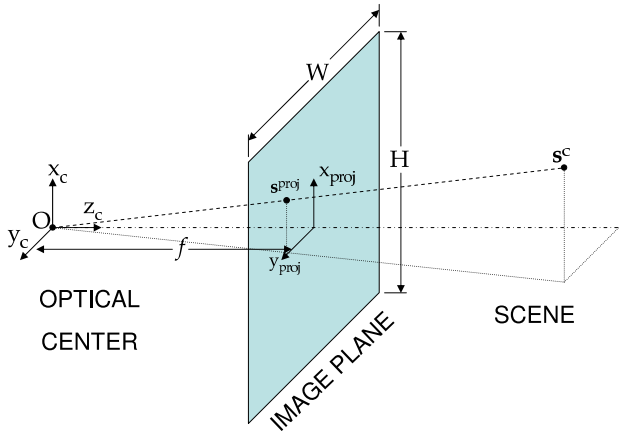

Figure 6: *Camera projection model. The pinhole camera model is represented by placing a virtual image plane one focal length in front of the optical center.*

optical center of the camera in the $\hat{z}^c$ direction. The pinhole camera model is discussed in more detail in [7].

Given the location of a feature relative to the navigation frame, $(\mathbf{t}^n)$, and the current position and orientation of the vehicle, $(\mathbf{p}^n, \mathbf{C}_b^n)$, the line-of-sight vector in the camera frame can be calculated as

$$\mathbf{s}^c = \left(\mathbf{C}_b^n \mathbf{C}_c^b\right)^T \left(\mathbf{t}^n - \mathbf{p}^n\right) \tag{9}$$

where $\mathbf{C}_c^b$ is the camera-to-body frame direction cosine matrix (DCM).

In the next section, the experimental simulation and flight test results are presented.

EXPERIMENT

The data collection system consisted of a consumer-grade MEMS IMU and two digital cameras. The IMU was a Microbotics MIDG consumer-grade MEMS unit (see [10]) which measured acceleration and angular rate at 50 Hz. The digital cameras were both Pixelink A-741 machine vision cameras which incorporated a global shutter feature and a Firewire interface. The lenses were wide-angle lenses with approximately 90 degrees field of view. The sensors were mounted on an aluminum bracket and calibrated using procedures similar to those described in [13]. Images were captured at approximately 2.5 Hz. The cameras were pointed down and forward at a 45-degree angle, respectively. For this paper, only the downward-pointing camera was used.

The data collection system was mounted on a C-12 *Huron* aircraft, owned by the USAF Test Pilot School (USAF TPS). A number of data collections were flown

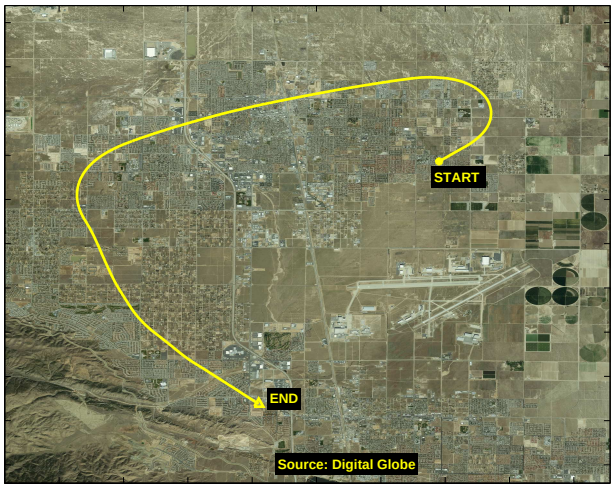

Figure 7: *Flight path for Palmdale data collection. The segment used in this research was flown over a combination of urban and desert terrain. Map imagery: ©Digital Globe, NextView.*

by USAF TPS in order to present the sensor with variations in terrain, airspeed, and altitude. For this test, a segment of flight data was used that consisted of a combination of urban and rural terrain (see Figure 7). Further variations in terrain and feature quality will be tested in future efforts. A GAINR-Lite (GLITE) Time-Space Positioning Information (TSPI) unit was mounted on the aircraft and served as the position, velocity, and orientation truth source. The GLITE system consists of a HG-1700 tactical-grade inertial sensor coupled with differentially-corrected pseudo-range measurements from a dual-frequency GPS receiver. The sensors are integrated using a post-flight smoother algorithm.

Simulation

A Monte Carlo simulation was used to evaluate the performance and stability of the GPS-aided inertial navigation algorithm both with and without image-aiding. The simulations were performed using a standard flight profile, based as closely as possible to the experimental flight data. The simulated trajectory was generated based on a semi-circular path with no overlapping portions. The trajectory was flown at approximately 1000 meters above relatively flat terrain above Palmdale, California. A five-minute segment of the profile was chosen with a combination of straight-and-level and turning portions.

For each Monte Carlo simulation, the inertial measurements and GPS measurements were generated with random errors consistent with the relevant error model. In addition, a collection of ground landmarks was generated using a digital terrain elevation database. In order to simulate the effects of uncertainty in the terrain model, a random elevation error was added to the landmark elevations. These simulated landmarks were then projected into the image plane and used to generate synthetic SIFT features, complete with localization and a randomized descriptor component. This method was chosen in order to stimulate the feature tracking algorithm as accurately as possible without going to the difficult step of generating simulated images with enough fidelity to exercise the feature tracking algorithm. As a result the Monte Carlo simulations should be an optimistic predictor of the true system performance as they correspond to a "best-case" scenario where there is virtually perfect feature tracking and a perfect camera distortion model. Thus, when the results are interpreted using this perspective, they can help to validate the concept and model, while serving as a lower bound performance expectation for this particular algorithm.

As mentioned previously, the target location error is a function of the position and attitude errors of the navigation system, camera boresight and uncorrected optical errors, and any errors in the terrain elevation database used to initialize the height estimate of the landmark. The horizontal target error can be thus approximated by expressing the horizontal target location, y_h, as:

$$y_h = p_h + h_v / \tan\theta \tag{10}$$

where p_h represents the horizontal position of the aircraft, h_v is the height of the aircraft above the terrain, and θ is the depression angle from horizontal to the target. Linearizing about the mean, represented using the overbar notation, results in the following first-order approximation

$$\delta y_h \approx \delta p_h + \frac{1}{\tan\bar{\theta}}\delta h_v - \frac{\bar{h}_v}{\sin^2\bar{\theta}}\delta\theta \tag{11}$$

Assuming independence, the horizontal target location variance, $\sigma^2_{y_h}$, is

$$\sigma^2_{y_h} = \sigma^2_{p_h} + \frac{1}{\tan^2\bar{\theta}}\sigma^2_{h_v} + \frac{\bar{h}_v^2}{\sin^4\bar{\theta}}\sigma^2_{\theta} \tag{12}$$

Examining Eq. 12 shows a dependence on the position and attitude uncertainty, as expected. Thus, for a given imaging scenario, the relative contribution of each error source can be determined. Assuming one meter of horizontal position error and three meters of vertical position error, the expected target location accuracy is a function of the height above terrain, elevation angle, and attitude errors. The resulting target location accuracy given variations of these parameters is shown in Figure 8.

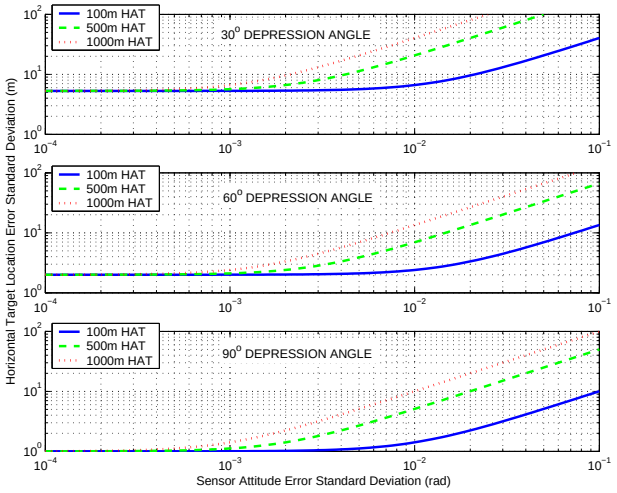

Figure 8: *Predicted Horizontal Target Location Error. The predicted horizontal target location error (TLE) is shown for depression angles of 30, 60, and 90 degrees. The effects of attitude accuracy and height above terrain demonstrates the critical importance of reducing attitude errors in order to improve target location accuracy. The figures assume a 1-meter horizontal and 3-meter vertical position error of the aircraft.*

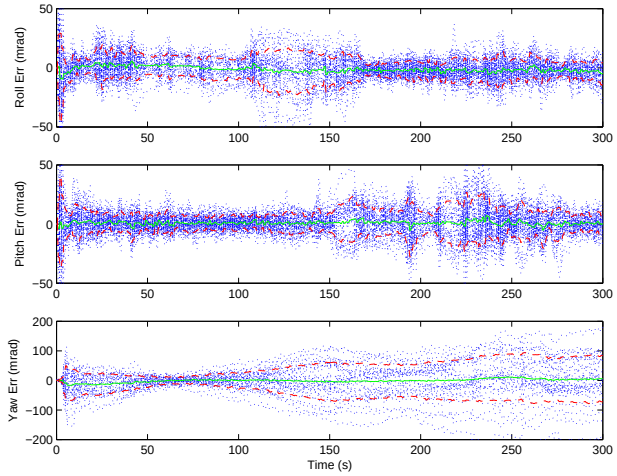

Figure 9: *Simulated attitude errors for consumer-grade GPS/IMU integration. As expected, the Monte Carlo simulation predicts relatively large heading errors. These errors would have a significant effect on target location accuracy.*

Simulation Results

The simulation results for the baseline GPS/IMU (no image aiding) case illustrates the difficulty in obtaining a high-quality target location from a UAV equipped with a low-cost inertial sensor. As shown in Figure 9, the attitude errors, especially in heading, have standard deviations on the order of 100 $mrad$. This results in a high target location errors, especially at longer slant ranges.

Incorporating the automated image-based feedback improves the attitude errors greatly. The resulting simulated attitude errors are shown in Figure 10. The standard deviation are on the order of 5 $mrad$, which is a significant improvement.

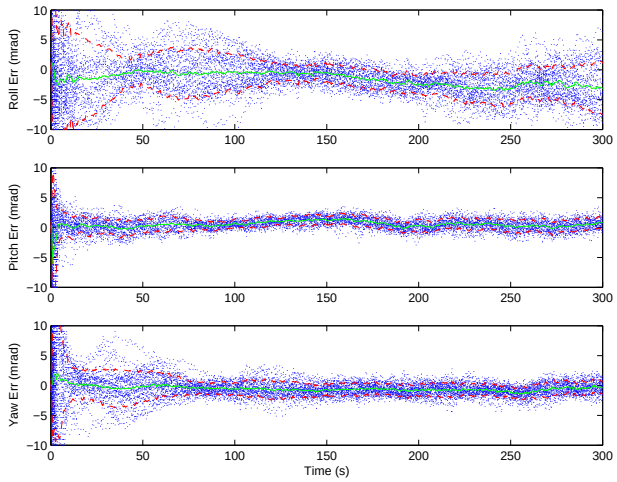

Figure 10: *Simulated attitude errors for consumer-grade GPS/IMU integration with image aiding using landmarks of opportunity. Incorporating the image-based measurements significantly improves the predicted attitude errors, resulting in an improvement in target location accuracy.*

Flight Test

The image-aided GPS/IMU algorithm was applied to a five-minute segment of the Palmdale, CA flight profile. The flight profile consisted of a semi-circular path, flown over a combination of urban and desert terrain. A sample image from the image-aiding algorithm illustrates the typical terrain observed by the sensor as well as a depiction of the camera field-of-view overlayed on the moving-map display (see Figure 11). For purposes of comparison, the navigation solution was calculated using the baseline GPS/IMU

Figure 11: *Sample feature track display from the Palmdale data collection. The currently-tracked features are depicted with red '+' symbols. Each feature is surrounded by a projection of the two-sigma error ellipse. In the right pane, the current features, quality, and field-of-view are overlayed on a moving-map display. Map imagery: ©Digital Globe, NextView.*

and using the image-aided GPS/IMU. The position and attitude errors are compared in Figures 12 and 13, respectively. A detailed view of the experimental attitude errors is shown in Figure 14. Although the deviations are larger than predicted by simulation, the estimate appears to be consistent with the filter's predicted one-sigma bounds.

As expected, the automatic image aiding significantly improves the attitude errors of the system. In addition, the position errors are consistent, which indicates the GPS measurements are dominating the positioning performance and that the image updates do not degrade this capability.

CONCLUSIONS

In this article, an algorithm was presented that improves the target location accuracy of a UAV equipped with a low-cost GPS/IMU and imaging system. The method is implemented recursively for online operation and only requires a terrain database. No *a prori* imagery is required over the area of operations. The system automatically selects and tracks stationary features in the field-of-view and uses these tracks to update the navigation state. The system was shown using a combination of simulation and flight test data to improve the attitude accuracy by an order of magnitude. This results in a corresponding improvement in target location accuracy.

The next step of this project is to build a smaller sen-

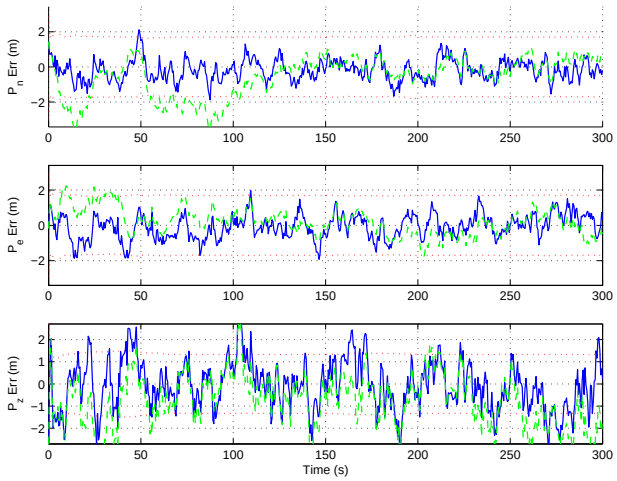

Figure 12: *Position errors for Palmdale flight test. The position errors were calculated for the GPS/IMU system with (represented by the dashed green trace) and without image aiding (represented by the solid blue trace). The dashed red lines indicate the one-sigma uncertainty bounds of the EKF for the non-image aided case. Note the image aiding does not significantly affect the positioning accuracy of the system.*

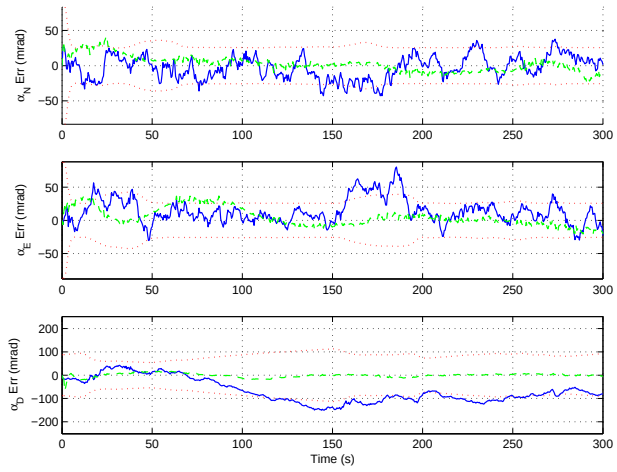

Figure 13: *Attitude errors for Palmdale flight test. The attitude errors were calculated for the GPS/IMU system with (represented by the dashed green trace) and without image aiding (represented by the solid blue trace). The dashed red lines indicate the one-sigma uncertainty bounds of the EKF for the non-image aided case. As predicted by simulation, the attitude errors are significantly improved by incorporating automatic image aiding to the GPS/IMU system.*

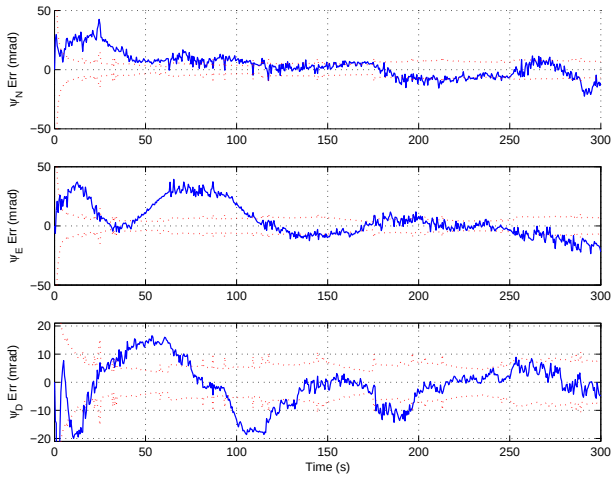

Figure 14: *Image-aided attitude errors for Palmdale flight test (detail). The attitude errors calculated using the image-aided GPS/IMU system show significant improvement over the non-image aided results. The estimates are reasonably consistent with the EKF predicted one-sigma bounds (red dashed lines).*

sor suitable for incorporation in our micro-UAV platform.

References

[1] Alison Brown, Bruce Bockius, Bruce Johnson, Heather Holland, and Dave Wetlesen. Flight test results of a video-aided gps/inertial navigation system. In *Proceedings of the 2007 ION GNSS Conference*, pages 1111–1117, 2007.

[2] Duane C. Brown. Close-range camera calibration. In *Proceedings of the Symposium on Close-Range Photogrammetry*, pages 855–866, January 1971.

[3] Jordan L. Fletcher, Michael J. Veth, and John F. Raquet. Real-time fusion of image and inertial sensors for navigation. In *Proceedings of the Institute of Navigation Annual Meeting*, pages 534–544, April 2007.

[4] Simon Haykin. *Kalman Filtering and Neural Networks*. John Wiley and Sons, Inc., New York, NY, 2001.

[5] Rui Hirokawa, Ryusuke Ohata, Takuji Ebinuma, and Tara Suzuki. A low cost gps/ins sensor for small uavs augmented with multiple gps antennas. In *Proceedings of the 2007 ION GNSS Conference*, pages 96–103, 2007.

[6] David G. Lowe. Distinctive image features from scale-invariant keypoints. *International Journal of Computer Vision*, 60(2):91–110, 2004.

[7] Yi Ma, Stefano Soatto, Jana Kosecka, and S. Shankar Sastry. *An Invitation to 3-D Vision*. Springer-Verlag, Inc., New York, New York, 2004.

[8] Peter S. Maybeck. *Stochastic Models Estimation and Control, Vol I*. Academic Press, Inc., Orlando, Florida 32887, 1979.

[9] Peter S. Maybeck. *Stochastic Models Estimation and Control, Vol II*. Academic Press, Inc., Orlando, Florida 32887, 1979.

[10] Microbotics, Inc. Midg 2 specifications. Specification, January 2007. URL: http://www.microboticsinv.com/.

[11] Bradford W. Parkinson and James J. Spilker. *Global Positioning System: Theory and Applications Volume IV*. American Institute of Astronautics and Aeronautics, Washington, DC, 1996.

[12] D.H. Titterton and J.L. Weston. *Strapdown Inertial Navigation Technology*. Peter Peregrinus Ltd., Lavenham, United Kingdom, 1997.

[13] Michael J. Veth and John F. Raquet. Alignment and calibration of optical and inertial sensors using stellar observations. In *Proceedings of ION GNSS 2005*, pages 2494–2503, September 2005.

[14] Michael J. Veth and John F. Raquet. Fusing low-cost imaging and inertial sensors for navigation. *Journal of the Institute of Navigation*, pages 11–20, 2007.

[15] Michael J. Veth, John F. Raquet, and Meir Pachter. Stochastic constraints for efficient image correspondence search. *IEEE Transactions on Aerospace Electronic Systems*, 42(3):973–982, July 2006.